

1 **Summertime tropospheric ozone assessment over the Mediterranean region using the**
2 **thermal infrared IASI/MetOp sounder and the WRF-Chem model**

3 **S. Safieddine¹, A. Boynard¹, P.-F. Coheur², D. Hurtmans², G. Pfister³, B. Quennehen¹, J. L.**
4 **Thomas¹, J.-C. Raut¹, K. S. Law¹, Z. Klimont⁴, J. Hadji-Lazarou¹, M. George¹ and C.**
5 **Clerbaux^{1,2}**

6 ¹Sorbonne Universités, UPMC Univ. Paris 06; Université Versailles St-Quentin; CNRS/INSU,
7 LATMOS-IPSL, Paris, France

8 ²Spectroscopie de l'Atmosphère, Chimie Quantique et Photophysique, Université Libre de
9 Bruxelles (U.L.B.), Brussels, Belgium

10 ³Atmospheric Chemistry Division, National Center for Atmospheric Research, Boulder,
11 Colorado, USA

12 ⁴International Institute for Applied Systems Analysis, Laxenburg A-2361, Austria

13
14
15
16
17
18
19
20
21
22
23
24

25 **Abstract**

26 Over the Mediterranean region, elevated tropospheric ozone (O_3) values are recorded, especially
27 in summer. We use the thermal Infrared Atmospheric Sounding Interferometer (IASI) and the
28 Weather Research and Forecasting Model with Chemistry (WRF-Chem) to understand and
29 interpret the factors and emission sources responsible for the high O_3 concentrations observed in
30 the Mediterranean troposphere. Six years (2008-2013) of IASI data have been analyzed and show
31 consistent maxima during summer, with an increase of up to 22% in the [0-8] km O_3 column in
32 the eastern part of the basin compared to the middle of the basin. We focus on summer 2010 to
33 investigate the processes that contribute to these summer maxima. Using two modeled O_3 tracers
34 (inflow to the model domain and local anthropogenic emissions), we show that between the
35 surface and 2 km, O_3 is mostly formed from anthropogenic emissions and above 4 km, is mostly
36 transported from outside the domain or from stratospheric origins. Evidence of stratosphere to
37 troposphere exchanges (STE) in the eastern part of the basin is shown, and corresponds with low
38 water vapor mixing ratio and high potential vorticity.

39 **1 Introduction**

40 Tropospheric ozone (O_3) is a greenhouse gas, air pollutant, and a primary source of the hydroxyl
41 radical OH, the most important oxidant in the atmosphere (Chameides and Walker, 1973;
42 Crutzen, 1973). Previous observations and studies have shown that tropospheric O_3 over the
43 Mediterranean exhibits a significant increase during summer time, especially in the east of the
44 basin (Kouvarakis et al., 2000; Im et al., 2011; Gerasopoulos et al., 2005, 2006a; Richards et al.,
45 2013; Zanis et al., 2014). Meteorological conditions such as frequent clear sky conditions (Fig.
46 1a) and high exposure to solar radiation (Fig. 1b) in summer enhance the formation of

47 photochemical O₃ due to the availability of its precursors. These precursors include carbon
48 monoxide (CO), peroxy radicals generated by the photochemical oxidation of volatile organic
49 compounds (VOCs) and nitrogen oxides (NO_x = NO + NO₂). Locally, the eastern part of the
50 basin is surrounded with megacities such as Cairo, Istanbul, and Athens that are large sources of
51 local anthropogenic emissions. The geographic location of the basin makes it a receptor for
52 anthropogenic pollution from Europe both in the boundary layer (Fig. 1c) and the mid-
53 troposphere (Fig. 1d). The threshold O₃ value for air quality standards for the European Union (of
54 daily maximum of running 8-hour mean values of 60 ppbv) is exceeded on more than 25 days per
55 year at a large number of stations across Europe, many of which are located to the south of
56 Europe in the Mediterranean basin (EEA, 2012). The dynamical processes of the summer
57 circulation over the Mediterranean were previously attributed to the Hadley cell considered as the
58 driver of the major subtropical dry zones. Rodwell and Hoskins (1996) argued that during the
59 June-August period, the zonal mean Hadley circulation has very little motion and cannot explain
60 the dry season of North Africa and the Mediterranean. Rodwell and Hoskins (1996; 2001)
61 suggested, through numerical simulations, that the Asian monsoon heating induces an
62 equatorially trapped Rossby wave to its west that interacts with the mid-latitude westerlies,
63 producing a region of adiabatic descent and triggering subsidence. Long term analysis of dP/dt
64 (units: Pa.s⁻¹, used to represent subsidence) shows indeed a positive enhancement over the
65 Mediterranean region (Ziv et al., 2004) making the South Asian monsoon a fundamental driver
66 of the summer circulation over the Eastern Mediterranean (Tyrlis et al., 2013). High O₃ values in
67 the Mediterranean troposphere in the literature are attributed to different sources: Lelieveld et al.
68 (2002) showed that in the upper troposphere, Asian pollution is transported from the east by the
69 monsoon across the Mediterranean tropopause into the lower stratosphere. Liu et al., (2011)
70 showed with long term model analysis that the dominant sources of O₃ in the Middle East

71 (including the Mediterranean) are the transport from Asia and local production. On the other
72 hand, Gerasopoulos et al. (2005) have shown that the mechanism that controls surface O₃
73 seasonal variability in the eastern basin during summer is mainly the transport from Europe.
74 Galani et al. (2003) detected with lidar measurements an increase of 10% of tropospheric O₃
75 between 4.5 and 6.5 km due to stratosphere to troposphere exchange events (STE). Zbinden et al.
76 (2013) using aircraft data from MOZAIC (Measurements of OZone and water vapour by in-
77 service Airbus airCraft programme) over 15 years (1994–2009), showed that the tropospheric O₃
78 columns in the east of the Mediterranean, reached a maximum reaching 43.2 DU during June-
79 July. This recorded maximum exceeds the maximum recorded for Beijing for the same period,
80 for example. Model calculation using WRF-Chem (Weather Research and Forecasting model
81 coupled with Chemistry) and EMEP (European Monitoring and Evaluation Programme) MSC-W
82 (Meteorological Synthesizing Centre-West) models of the Eastern Mediterranean during heat
83 waves in 2007 showed that the daily maximum near surface O₃ is mostly sensitive to
84 anthropogenic emissions of O₃ precursors (Hodnebrog et al., 2012). Im et al. (2011) found that
85 the near surface ozone mixing ratios increases almost linearly with temperature by 1.0±0.1 ppb
86 O₃ per Kelvin. STE processes can affect the tropospheric O₃ budget and impact air quality if
87 transported to the boundary layer (Fiore et al., 2002). Stratospheric intrusions have been detected
88 in the Mediterranean region, especially to the east side (Galani et al., 2003; Zanis et al., 2014),
89 because it lies to the south of the North Hemisphere polar jet flowing over mid-latitudes (Stohl et
90 al., 2000; Gerasopoulos et al., 2001). Understanding the factors that contribute to the O₃ maxima
91 is important for developing control measures and prevents pollution build up. In this study we
92 analyze O₃ and its sources at different altitudes in the Mediterranean troposphere. Section 2
93 introduces the model and observations data sets used in this study. In section 3, we analyze six
94 years (2008-2013) of IASI tropospheric [0-8] km O₃ column seasonal variation above the whole

95 Mediterranean basin as well as at 15°E and 30°E, representative of what we henceforth refer as
96 “middle of the basin” and “east of the basin” respectively. In section 4 we focus on summer
97 2010, as an example year, and validate the WRF-Chem model simulation with surface O₃ and
98 IASI data, and then use the WRF-Chem model to assess the sources of O₃ in the troposphere. In
99 section 5, we use IASI and WRF-Chem free tropospheric O₃ data to investigate potential
100 stratosphere to troposphere exchange events. Discussion and conclusions are given in section 6.

101

102 **2 Model and observational data**

103 **2.1 WRF-Chem model**

104 In this study, we use the regional chemistry transport model WRF-Chem, Version 3.2 (Grell et
105 al., 2005) to assess the O₃ budget and spatio-temporal variability of O₃ over the Mediterranean
106 during summer 2010. The model domain shown in Fig. 2a is over Europe and the Mediterranean
107 basin, the latter being the focus of this study (Fig. 2b). The horizontal resolution is of 50 km x 50
108 km and the vertical resolution is of 28 levels between the surface and 10 hPa. The meteorological
109 initial and boundary conditions are based on the National Centers for Environmental Prediction
110 (NCEP) Final (FNL) analyses with analysis nudging for wind, temperature, and humidity applied.
111 Fields are provided every 6 hours with 1° horizontal resolution and 27 vertical levels from the
112 surface up to 10 hPa. The chemical initial and boundary conditions, spatially and temporally
113 varying (6 hours), are constrained by global chemical transport simulations from MOZART-
114 4/GEOS-5 with 1.9° x 2.5° horizontal resolution (Emmons et al., 2010a). The WRF-Chem gas-
115 phase chemical mechanism is that from Model for Ozone and Related Chemical Tracers, version
116 4 (MOZART-4) (Emmons et al., 2010a), which is coupled to the aerosol scheme Goddard
117 Chemistry Aerosol Radiation and Transport (GOCART) model (Chin et al., 2002). The model
118 also includes anthropogenic and fire emissions that are calculated off-line. The anthropogenic

119 emissions used within the WRF-Chem model were developed in the frame of the ECLIPSE
120 European project using the Greenhouse gas and Air pollution Interactions and
121 Synergies (GAINS) model. In addition to the ECLIPSE V4.0 anthropogenic emissions, ship
122 emissions from the RCP 6.0 scenario (Fujino et al., 2006; Hijioka et al., 2008) were used.
123 Biomass burning emissions are obtained from the Fire Inventory from NCAR (FINN V1)
124 (Wiedinmyer et al., 2011). Biogenic emissions are calculated online from the Model of Emissions
125 of Gases and Aerosols from Nature (MEGAN) (Guenther et al., 2006). The WRF-Chem
126 simulation outputs are saved every 2 hours from 1 June 2010 until 31 August 2010.

127 In this study, we use a tagging method for O₃ (Emmons et al., 2012), which has been applied in
128 global models for diagnosing contributions for individual sources to O₃ (e.g. Lamarque et al.,
129 2005; Pfister et al., 2006, 2008; Emmons et al., 2010b; Wespes et al., 2012), and in other global
130 and regional chemical transport models (Ma et al., 2002; Hess and Zbinden, 2013). Recently, this
131 scheme was used for the first time in the WRF-Chem model to quantify the contribution of
132 transport on surface O₃ over California (Pfister et al., 2013). Here, we apply this scheme to keep
133 track of the contribution of O₃ within the WRF-Chem domain. To determine O₃ sources, tagged
134 NO_x is traced through the odd nitrogen species (e.g. PAN, HNO₃, organic nitrates) to account for
135 NO_x recycling (Emmons et al., 2012). Two separate tracer runs were conducted with the same
136 emissions, initial, and boundary conditions. In the first one, O_{3-ANTHRO} tracer accounts for the
137 anthropogenic regional tagged NO_x, while the second one O_{3-INFLOW} tracer accounts for tagged O₃
138 as well as all nitrogen species at the lateral boundaries of the regional model domain. O_{3-INFLOW}
139 tracer includes O₃ and O₃ precursors from all natural (including lightning and stratospheric O₃)
140 and anthropogenic sources outside the regional modeling domain. Within the regional modeling
141 domain, O_{3-INFLOW} undergoes transport and chemical processes, but is not produced from sources
142 other than from reactions including the tagged species. Since in this version of WRF-Chem the

143 stratospheric O₃ is controlled by the lateral boundaries, O₃ from stratospheric intrusions within
144 the regional domain would be labeled as O_{3-INFLOW} as well. More details about the tagging
145 scheme are provided in Emmons et al. (2012). Two more tracers are available to complete the O₃
146 budget: O₃ from biogenic sources and O₃ from fires. Given that their contribution to the total
147 budget in comparison with O_{3-INFLOW} and O_{3-ANTHRO} tracers is small (<10%), they are analyzed
148 together in this study as “residuals” to the total budget and their contribution is defined as 100%-
149 $(O_{3-ANTHRO}\% + O_{3-INFLOW}\%)$. We focus our analysis on summer 2010, which corresponds to the
150 year of the anthropogenic emission inventory used in the model. During July-August 2010, the
151 Russian heat wave occurred that caused severe fires with high O₃ and O₃ precursors’ emissions
152 that were probably transported to the Mediterranean region, and will be further investigated in
153 this study.

154 **2.2 EMEP data**

155 The EMEP (European Monitoring and Evaluation Programme) O₃ hourly data
156 (<http://ebas.nilu.no/>) are used to validate the WRF-Chem model at the surface. All ozone
157 measurements within EMEP are done by UV monitors. In this study, measurements at 8 ground
158 rural background sites during the summer of 2010 are used. Details on the EMEP observation
159 system can be found in Hjellbrekke et al. (2012). The geographic locations of the 8 stations used
160 for validation are plotted in Fig. 2 and the corresponding details are listed in Table 1. Two more
161 station data were available, GR01-Aliartos (38.37°N, 23.11°E) and IT01-Montelibretti (42.1°N,
162 12.63°E). We disregarded the data from these stations because they show strong diurnal variation
163 of 80-90 ppbv amplitude, and recurrent near zero O₃ concentrations throughout the period of the
164 study, and were thus considered unreliable.

165 **2.3 IASI satellite measurements**

167 On board of the MetOp platforms, IASI was launched in October 2006 (IASI-1) and September
168 2012 (IASI-2). It has been sounding operationally the atmosphere since June 2007 (IASI-1) and
169 January 2013 (IASI-2). IASI is a nadir looking Fourier transform spectrometer that probes the
170 Earth's atmosphere in the thermal infrared spectral range between 645 and 2760 cm^{-1} , with a
171 spectral resolution of 0.5 cm^{-1} (apodized) and 0.25 cm^{-1} spectral sampling. Global distributions of
172 O_3 vertical profiles are retrieved in near real time using a dedicated radiative transfer and retrieval
173 software for the IASI O_3 product, the Fast Optimal Retrievals on Layers for IASI (FORLI- O_3)
174 (Hurtmans et al., 2012). The IASI FORLI- O_3 observations are selected for scenes with cloud
175 coverage below 13%, and with RMS of the spectral fit residual lower than $3.5 \times 10^{-8} \text{ W/cm}^2 \cdot \text{sr} \cdot \text{cm}^{-1}$.
176 Details about the chemical components that can be measured by IASI can be found in Clerbaux
177 et al. (2009), Coheur et al. (2009), Turquety et al. (2009), and Clarisse et al. (2011). IASI has the
178 highest O_3 sensitivity in the mid to upper troposphere (Safieddine et al., 2013). Figure 3 shows
179 the partial column averaging kernel function for two specific observations above land and sea
180 during June 2010. It can be seen that the sensitivity to the O_3 profile is maximal around 4-10 km
181 for both observations. IASI sensitivity near the surface is usually limited above the sea, as seen
182 on the right panel of Fig. 3, and better over land as seen in the left panel, and with corresponding
183 better thermal contrast (7.8° above land, and 1.2° above sea). In fact, IASI is able to detect several
184 pollutants (e.g. carbon monoxide, ammonia, sulfur dioxide and ammonium sulfate aerosols),
185 especially when large thermal contrast is combined with stable meteorological conditions leading
186 to the accumulation of pollutants near the surface (Boynard et al., 2014).

187 **3 Tropospheric O_3 seasonal variation as seen by IASI**

188 To investigate the seasonal behavior of tropospheric O_3 above the Mediterranean, we plot in Fig.
189 4 the [0-8] km partial tropospheric O_3 column as seen by IASI, during 2008 to 2013. The data
190 were averaged seasonally and daytime observations were used since the information content of

191 IASI-O₃ data is shown to be higher during the day (Clerbaux et al., 2009). We observe a similar
192 tropospheric O₃ seasonal behavior each year. The weakest values are observed in winter (DJF)
193 and autumn (SON), when solar activity is minimal. Increasing values in spring (MAM) are due to
194 the increase of O₃ production from photochemistry, buildup of winter O₃ and its precursors,
195 transport, and/or from O₃ of stratospheric origin integrating into the troposphere. The [0-8] km
196 column reaches a maximum in summer (JJA) due to high photochemical O₃ production,
197 horizontal transport into the region, or stratosphere to troposphere exchange, all of which will be
198 investigated in detail in the following sections. Richards et al. (2013) detected a similar spatial
199 distribution with the Global Ozone Monitoring Experiment-2 (GOME-2) during summers of
200 2007 and 2008, with values exceeding 32 DU at the east of the basin for the [0-6] km O₃ column.
201 To investigate further the higher values detected to the east of the basin, we analyze longitudinal
202 transects of 1° width along 15°E (representing the middle of the basin) and 30°E (representing the
203 east of the basin), and marked in orange in Fig. 2.
204 Figure 5 shows that during the period of 2008 to 2013, the summers in the east of the basin,
205 notably at 30°E (plotted in red) are marked by elevated tropospheric [0-8] km O₃ values. The
206 difference between the two O₃ columns at the 2 different longitudes was highest (4.7 DU-22 %)
207 during June 2012. The highest recorded values were up to 30 Dobson units (DU) in July 2010 at
208 30°E. This period coincides with the 2010 Russian heat wave (Schubert et al., 2011) that caused
209 severe fires with high O₃ precursors emissions (R'Honi et al., 2013). Further discussion is
210 provided in section 4.2

211
212
213
214

215 **4 O₃ budget from the WRF-Chem model during summer 2010**

216 From this section onwards, we focus our analysis on summer 2010, the year of the anthropogenic
217 emission inventory used in the model. We evaluate the model then we discuss the O₃ budget at
218 different altitude levels in the Mediterranean troposphere.

219 **4.1 Model evaluation: comparison to EMEP and IASI**

220 The model is evaluated by comparing O₃ concentrations with surface O₃ data from the EMEP
221 stations (section 2.2), then free tropospheric O₃ data from IASI (section 2.3).

222 **4.1.1 Comparison to EMEP surface monitoring stations**

223 Linear spatial interpolation was applied to WRF-Chem data in order to correlate the model
224 outputs and the EMEP data that were averaged every 2 hours to coincide with the model run
225 output data. Figure 6 shows the individual time series of the data of the 8 stations used for the
226 validation. Table 2 shows the individual O₃ correlation and bias between WRF-Chem and the
227 EMEP for each of the stations used in this study during JJA 2010. The model simulates the
228 surface O₃ with a correlation ranging from 0.41 (ES06) to 0.80 (ES12) and a mean value of 0.52.
229 Figure 6 and Table 2 show that the model reproduces reasonably well the average amplitude of
230 the daily cycle seen in the observation. For all stations except ES06 and ES10, the model
231 underestimates the ground observation during the summer period with a mean normalized bias
232 between -23.9% to -6.4%. The biases reported may be due to the resolution of the model resulting
233 in a grid of around 50 km around the EMEP rural sites which may include other surface O₃
234 contributions. Other possible reasons include difficulties in simulating local flow patterns due to
235 topography and land-sea circulation, as well as uncertainties in emissions and NO_x concentrations
236 (Pfister et al., 2013). Our results compare well with the study by Tuccella et al. (2012) that
237 compared WRF-Chem to 75 EMEP stations over Europe during 2007, and found that hourly O₃
238 exhibit a correlation with observations ranging from 0.38 to 0.83. The largest discrepancy

239 observed, with modeled O₃ values larger than 80 ppbv, is for the station ES06-Mahon (39.87°N,
240 4.32°E), which might be due a particular uncertainty in the model emissions or dry deposition
241 over this area.

242 **4.1.2 Comparison to IASI observations**

243 Averaged data for summer 2010 are used for the comparison of WRF-Chem and IASI O₃ [4-10]
244 km free tropospheric column. The modeled profile is first linearly interpolated to the time and
245 location of the retrieval. Then, the averaging kernels associated with each IASI measurement and
246 its *apriori* profile are applied to the interpolated modeled profile (of around 7 layers between 4
247 and 10 km). Figure 7 shows the spatial distribution of the [4-10] km integrated IASI and WRF-
248 Chem model O₃ column along with the relative differences. We chose to analyze this part of the
249 atmosphere in particular because IASI has a better sensitivity between 4 and 10 km over both
250 land and water as shown in Fig. 3. The model reproduces well the spatial patterns seen by IASI
251 during summer (JJA) 2010, with a correlation coefficient of about 0.93 and a summertime mean
252 bias of 6.1 DU (25%) (not shown). The model underestimation of the [4-10] km O₃ column might
253 due to the difficulties in resolving the high O₃ concentrations observed in transported plumes
254 over large distances (Pfister et al., 2013). On the other hand, the high discrepancies seen over
255 northern Africa, might be due to IASI poor spectral fits above surfaces with sharp emissivity
256 variations particularly above the desert (Hurtmans et al., 2012), leading to a possible
257 overestimation of the real profile. We analyzed the IASI total retrieval error for the [4–10] km
258 partial column and we found that it is on average around 7% in the model domain, and between 7
259 and 12% where the discrepancies between the model and IASI are the highest.

260 **4.2 Origins of boundary layer O₃ over the Mediterranean**

261 Modeled O₃ concentrations are illustrated in Fig. 8 (a-c) at the surface, 1 and 2 km during JJA
262 2010. At the surface, modeled O₃ exhibits the highest values downwind the European continent.
263 At 1 and 2 km the whole eastern part of the basin is characterized by high O₃ mixing ratios. In
264 order to investigate possible sources of high O₃, we run the model with 2 different tracers of
265 pollution: O_{3-ANTHRO} and O_{3-INFLOW} as described in section 2.1. O_{3-ANTHRO} (Fig. 8 d-f) assesses the
266 possible anthropogenic contribution of O₃ at different altitudes, while O_{3-INFLOW} (Fig. 8 g-i),
267 provides an estimate of transport of O₃ including the stratosphere. The residual plots plotted in
268 panels (j-l) show the completion of the O₃ budget, and represent the O₃ contribution from fires
269 and biogenic sources. These plots show that the residual contribution is between 0 and 10%
270 inferring that the O_{3-ANTHRO} and O_{3-INFLOW} combined are responsible of 90 to 100% of the total O₃
271 budget over the model domain, at the different altitudes of Fig. 8 and 9. The surface shows a high
272 contribution for the anthropogenic emission tracer (O_{3-ANTHRO} > 85%), with almost zero
273 contribution of the inflow tracer. This shows the importance of local emissions to the O₃ surface
274 concentration. At 1 km, the highest contribution is also for the anthropogenic tracer (up to 75-
275 80%), whereas the result is mixed at 2 km between the 2 tracers (around 50-60% for O_{3-ANTHRO}
276 and 40-50% for O_{3-INFLOW}), suggesting that up to 50% of the O₃ available at 2 km is being
277 transported. The rest of the O₃ plotted in the residual plots (panels j-l) and decreasing with
278 altitude is suggested to be from fire sources, as the extended domain (Fig 2a) used in the study
279 includes parts of the region hit by the Russian fires of summer 2010.

280 281 **4.3 Origins of free tropospheric O₃ over the Mediterranean**

282 O₃ concentrations at 4, 6 and 8 km in Fig. 9 (a-c) show that the eastern part of the basin is subject
283 to much higher O₃ values, reaching up to 100 ppbv between 6 and 8 km (see further discussion in
284 section 5). The anthropogenic contribution decreases with altitude, whereas the O₃ inflow

285 contribution increases. The northeastern corner of the modeled domain in panels (d-f) show
286 anthropogenic contribution between 20 and 40%. This might be due to important vertical
287 transport and mixing in the free troposphere. These values can be correlated with the O₃ residuals
288 plotted in panels (j-l). These panels show an O₃ signature in the north eastern corner of the
289 domain. This signature is probably related to the emitted O₃ precursors from fires sources in the
290 model domain (Fig. 2) and lifted to the upper troposphere due to convective movements during
291 the Russian fires of summer 2010. We can also suppose that certain anthropogenic O₃ precursors,
292 like NO_x, near the fire sources were also transported with the same convective movements to the
293 same part of the domain and contributed eventually to the production of anthropogenic O₃ in that
294 region. Panels (g-i) show that 70 to 100% of the available O₃ between 4 and 8 km does not come
295 from local sources. The high values are likely due to long-range transport of pollution from
296 outside the study region or transport of air masses from the stratosphere that we will discuss in
297 the following section. The low values recorded in the residual plots in panels (j-l) show that the
298 O₃ budget in the free troposphere over this region is controlled almost exclusively by local
299 anthropogenic sources and transport.

300

301 **5 WRF-Chem and IASI detection of stratosphere-troposphere exchange events**

302 Figures 4, 5 and Fig. 9 (a-c) showed that the eastern part of the Mediterranean basin in summer is
303 subject to high O₃ mixing ratios at 4, 6 and 8 km. In order to further investigate the sources and
304 processes responsible for these enhancements, modeled and observed IASI O₃ vertical profiles in
305 the troposphere were examined, during summer 2010, to try to detect possible stratosphere to
306 troposphere exchange (STE) events.

307 Figure 10 shows the tropospheric O₃ vertical distributions along 15°E (mid-Mediterranean) and
308 30°E (eastern Mediterranean) for IASI (panels a and b) and WRF-Chem, smoothed with the IASI

309 averaging kernels (panels c and d) for JJA 2010. Between 4 and 8 km, panels (b) and (d) show
310 higher values of O_3 in the eastern part of the basin ($30^\circ E$) with concentrations ranging between 50
311 and 100 ppbv for IASI and 40 to 100 ppbv for WRF-Chem (WRF-Chem underestimates IASI as
312 shown in Fig. 7).

313 Since stratospheric intrusions within the regional domain are included in the $O_{3-INFLOW}$ tracer, it is
314 useful to use other stratospheric tracers to distinguish the transport from the stratosphere. The
315 potential vorticity (PV) and the water vapor mixing ratio (Q_{vap}) measurements can be used as
316 markers of transport from the upper troposphere-lower stratosphere (UTLS) to the troposphere:
317 elevated O_3 and PV, and low Q_{vap} values, would indicate that high free troposphere values are
318 due to downward transport from the UTLS (Holton et al., 1995). Here, we study PV and Q_{vap} at
319 4, 6, and 8 and 10 km calculated from the WRF-Chem model run parameters. Figure 11 shows
320 that starting 4 km, higher PV and lower Q_{vap} values start to develop to the east of the basin. At 8
321 and 10 km, the highest PV values (1.5 to 2 pvu) (potential vorticity unit, $1\text{pvu} = 10^{-6} \text{ m}^2 \text{ K kg}^{-1} \text{ s}^{-1}$)
322 1), and the lowest Q_{vap} values (0-0.10 g.kg^{-1}) are recorded to the east of the basin, in comparison
323 with low PV values in the mid and to the west of the basin (0.5-1), with high Q_{vap} values (0.1-
324 0.15). The high PV/low Q_{vap} values to the east are in accordance with Fig. 9 and 10, strongly
325 suggesting that this part of the basin is subject to transport from the UTLS into the free
326 troposphere. In fact, at $30^\circ E$ and around $37^\circ N$ - $39^\circ N$ (panels b and d of Fig. 10) both IASI and the
327 model suggest a stratospheric intrusion. It corresponds to PV values between 1.4 and 2 pvu at 8
328 km and Q_{vap} values around 0.05 g.kg^{-1} . In a recent study, Zanis et al. (2014) using 12 year
329 climatology (1998-2009) of the ERA-interim reanalysis, also detected frequent events of STE
330 with PV ranging between 0.4 and 1.4 pvu and specific humidity values between 0.01 and 2 g.kg^{-1}
331 between 700 and 250 hPa during July and August to the east of the basin, in accordance with our
332 results for summer 2010 at 4, 6 and 8 km.

333 6 Discussion and conclusions

334 Six years of tropospheric O₃ observations provided by the IASI mission above the Mediterranean
335 are shown. Tropospheric [0-8] km O₃ columns show a consistent seasonal behavior over the
336 period 2008-2013 with pronounced maxima in summer with higher values to the east of the
337 basin. A complementary study by Doche et al. (2014) using IASI data at 3 km height, also
338 showed 6 years recurrent O₃ summer maxima in July to the east of the basin. Since IASI has a
339 lower sensitivity in the lower troposphere and above the sea, anthropogenic emission contribution
340 to the boundary layer O₃ is not well captured by the instrument. However, IASI is able to detect
341 in the free to upper troposphere, where its sensitivity is the highest, high tropospheric O₃ values
342 to the east of the basin during the 6 years. Focusing on summer 2010, we use IASI and the
343 regional chemical transport model WRF-Chem to interpret these maxima. A tagging scheme is
344 used to keep track of O₃ from anthropogenic sources in the domain (O_{3-ANTHRO}) and O₃ from
345 inflow at the domain boundaries and stratosphere (O_{3-INFLOW}). Our results show that transport
346 plays an essential role in the O₃ budget over the Mediterranean troposphere and that summer O₃
347 maxima over the region are recorded especially in the eastern part of the basin. Even though high
348 local anthropogenic emissions are responsible to 60-100% of O₃ in the boundary layer (surface-2
349 km), as demonstrated by the anthropogenic O₃ tracer of the WRF-Chem model, above 2 km, O₃ is
350 mainly transported. Kalabokas et al. (2007, 2013) showed that the highest ozone concentrations
351 in the low troposphere are associated with large-scale subsidence of ozone-rich air masses from
352 the upper troposphere. However, Zanis et al., (2013) using model simulations reported, that at the
353 low troposphere, long distance transport and local photochemical processes dominate. In the free
354 troposphere, WRF-Chem shows that vertical and lateral transport of O₃ take place represented by
355 the O_{3-INFLOW} tracer which is responsible for 70-100% of O₃ at 4, 6 and 8 km. In the Eastern

356 Mediterranean, Roelofs et al. (2003) showed important contributions to elevated O₃ in the middle
357 troposphere by transport from the stratosphere. More recently, Hess and Zbinden (2013) showed
358 that stratospheric inter-annual O₃ variability drives significantly the O₃ variability in the middle
359 troposphere, between 30° and 90°N but not the overall trend which is largely affected by transport
360 processes. The increase in O₃ seen by the model and the IASI instrument in the eastern part of the
361 Mediterranean basin suggests that stratosphere to troposphere exchange (STE) events contribute
362 to elevated ozone in the upper free troposphere. This is further shown in the WRF-Chem
363 simulations that predict elevated potential vorticity (PV) and water vapor mixing ratio (Q_{vap}) over
364 the same region. This result is in agreement with many previous studies e.g. Butkovic et al.
365 (1990); Varotsos and Cracknell (1993); Kalabokas and Bartzis (1998); Kalabokas et al. (2000,
366 2007); Kouvarakis et al.(2000); Lelieveld et al.(2002); Sprenger and Wernli (2003); Papayannis
367 et al. (2005); Gerasopoulos et al. (2006b); Akritidis et al. (2010); Zanis et al. (2013); Doche et al.
368 (2014) that have shown the occurrence of STE events in the eastern Mediterranean region in
369 summer. Since O₃ maxima have the potential to strongly impact regional air quality and climate
370 (e.g. Hauglustaine and Brasseur, 2001), the present study further demonstrate the importance of
371 quantifying and analyzing O₃ and its sources at different altitudes in the atmosphere. Quantifying
372 long term trends and a distinction between the different sources is crucial. This should be
373 possible with observations and model runs over longer time scales with additional tracers to
374 identify all O₃ sources.

375
376 *Acknowledgments.* IASI is a joint mission of EUMETSAT and the Centre National d'Etudes
377 Spatiales (CNES, France). The IASI L1 data are distributed in near real time by EUMETSAT
378 through the EumetCast system distribution. The authors acknowledge the French Ether
379 atmospheric database (www.pole-ether.fr) for providing the IASI L1C data and L2 temperature

380 data. This work was undertaken under the auspices of the O3M-SAF project of the EUMETSAT
381 and supported by the European Space Agency (ozone CCI project). The French scientists are
382 grateful to CNES and Centre National de la Recherche Scientifique (CNRS) for financial support.
383 The research in Belgium is funded by the Belgian State Federal Office for Scientific, Technical
384 and Cultural Affairs and the European Space Agency (ESA Prodex arrangement). P.F. Coheur is
385 Senior Research Associate with F.R.S-FNRS. Support is also acknowledged from the EU FP7
386 ECLIPSE (Evaluating the Climate and Air Quality Impacts of Short-Lived Pollutants) project
387 (no. 282688).

388 **References**

- 389 Akritidis, D., Zanis, P., Pytharoulis, I., Mavrakis, A., and Karacostas, T.: A deep stratospheric
390 intrusion event down to the earth's surface of the megacity of Athens, *Meteorol. Atmos. Phys.*,
391 109, 9–18, doi:10.1007/s00703-010-0096-6, 2010.
392
- 393 Bolle, H.-J. Ed., *Mediterranean Climate: Variability and Trends*, Springer-Verlag, Berlin, 2002.
394
- 395 Boynard, A., Clerbaux, C., Clarisse, L., Safieddine, S., Pommier M., Van Damme, M., Bauduin,
396 S., Oudot, C., Hadji-Lazaro, J., Hurtmans, D., Coheur, P.-F.: First simultaneous space
397 measurements of atmospheric pollutants in the boundary layer from IASI: a case study in the
398 North China Plain, *Geophys. Res. Lett.*, 41, 645–651 doi:10.1002/2013GL058333, 2014.
399
- 400 Butkovic, V., Cvitas, T., and Klasinc, L.: Photochemical ozone in the Mediterranean, *Sci. Total*
401 *Environ.*, 99, 145–151, doi:10.1016/0048-9697(90)90219-k, 1990.
402
- 403 Chameides, W. and Walker, J. C. G.: A photochemical theory of tropospheric ozone, *J. Geophys.*
404 *Res.*, 78, 8751–8760, 1973.
405
- 406 Chin, M., Ginoux, P., Kinne, S., Torres, O., Holben, B. N., Duncan, B. N., Martin, R. V., Logan,
407 J. A., Higurashi, A., and Nakajima, T.: Tropospheric aerosol optical thickness from the GOCART
408 model and comparisons with satellite and Sun photometer measurements, *J. Atmos. Sci.*, 59,
409 461–483, 2002.
410
- 411 Clarisse, L., R'Honi, Y., Coheur, P.-F., Hurtmans, D., and Clerbaux, C.: Thermal infrared nadir
412 observations of 24 atmospheric gases, *Geophys. Res. Lett.*, 38, L10802,
413 doi:10.1029/2011GL047271, 2011.
414

415 Clerbaux, C., Boynard, A., Clarisse, L., George, M., Hadji-Lazaro, J., Herbin, H., Hurtmans, D.,
416 Pommier, M., Razavi, A., Turquety, S., Wespes, C., and Coheur, P.-F.: Monitoring of
417 atmospheric composition using the thermal infrared IASI/MetOp sounder, *Atmos. Chem. Phys.*,
418 9, 6041-6054, doi:10.5194/acp-9-6041-2009, 2009.

419 Coheur, P.-F., Clarisse, L., Turquety, S., Hurtmans, D., and Clerbaux, C.: IASI measurements of
420 reactive trace species in biomass burning plumes, *Atmos. Chem. Phys.*, 9, 5655–5667,
421 <http://www.atmos-chem-phys.net/9/5655/2009/>, 2009.

422

423 Crutzen, P. J.: A discussion of the chemistry of some minor constituents in the stratosphere and
424 troposphere, *Pure Appl. Geophys.*, 106-108, 1385, 1973.

425

426 Doche, C., Dufour, G., Foret, G., Eremenko, M., Cuesta, J., Beekmann, M., and Kalabokas, P.:
427 Summertime tropospheric ozone variability over the Mediterranean basin observed with IASI,
428 *Atmos. Chem. Phys. Discuss.*, 14, 13021-13058, doi:10.5194/acpd-14-13021-2014, 2014.

429

430 EEA: Air Quality in Europe – 2012 Report, European Environment Agency, ISBN 978-92-9213-
431 328-3, Luxembourg, Office for Official Publications of the European Union, doi:10.2800/55823,
432 2012.

433

434 Emmons, L. K., Walters, S., Hess, P. G., Lamarque, J.-F., Pfister, G. G., Fillmore, D., Granier,
435 C., Guenther, A., Kinnison, D., Laepple, T., Orlando, J., Tie, X., Tyndall, G., Wiedinmyer, C.,
436 Baughcum, S. L., and Kloster, S.: Description and evaluation of the Model for Ozone and Related
437 Chemical Tracers, version 4 (MOZART-4), *Geosci. Model Dev.*, 3, 43-67, 2010a.

438

439 Emmons, L. K., Apel, E. C., Lamarque, J.-F., Hess, P. G., Avery, M., Blake, D., Brune, W.,
440 Campos, T., Crawford, J., DeCarlo, P. F., Hall, S., Heikes, B., Holloway, J., Jimenez, J. L.,
441 Knapp, D. J., Kok, G., Mena-Carrasco, M., Olson, J., O’Sullivan, D., Sachse, G., Walega, J.,
442 Weibring, P., Weinheimer, A., and Wiedinmyer, C.: Impact of Mexico City emissions on
443 regional air quality from MOZART-4 simulations, *Atmos. Chem. Phys.*, 10, 6195–6212,
444 doi:10.5194/acp-10-6195-2010, 2010b.

445

446 Emmons, L., Hess, P., Lamarque, J., and Pfister, G.: Tagged ozone mechanism for MOZART-4,
447 CAM-chem and other chemical transport models, *Geosci. Model Dev.*, 5(6), 1531–1542,
448 doi:10.5194/gmd-5-1531-2012, 2012.

449

450 Fiore, A. M., Jacob, D. J., Bey, I., Yantosca, R. M., Field, B. D., Fusco, A. C., and Wilkinson, J.
451 G.: Background ozone over the United States in summer: Origin, trend, and contribution to
452 pollution episodes, *J. Geophys. Res.*, 107(D15), 4275, doi:10.1029/2001JD000982, 2002.

453

454 Fujino, J., Nair, R., Kainuma, M., Masui, T., and Matsuoka, Y.: Multi-gas mitigation analysis on
455 stabilization scenarios using AIM global model, multigas mitigation and climate policy, *Energ. J.*,
456 27, 343–353, 2006.

457

458 Galani, E., Balis, D., Zanis, P., Zerefos, C., Papayannis, A., Wernli, H., and Gerasopoulos, E.:
459 Observations of stratosphere-troposphere transport events over the eastern Mediterranean using a
460 ground-based lidar system, *J. Geophys. Res.*, 108, D128527, doi:10.1029/2002JD002596, 2003.

461
462 Gerasopoulos, E., Zanis, P., Stohl, A., Zerefos, C. S., Papastefanou, C., Ringer, W., Tobler, L.,
463 Huebener, S., Kanter, H. J., Tositti, L., and Sandrini, S.: A climatology of ⁷Be at four high-
464 altitude stations at the Alps and the Northern Apennines, *Atmos. Environ.*, 35, 6347–6360, 2001.
465
466 Gerasopoulos, E., Kouvarakis, G., Vrekoussis, M., Kanakidou, M., Mihalopoulos, N.: Ozone
467 variability in the marine boundary layer of the Eastern Mediterranean based on 7-year
468 observations, *J. Geophys. Res.*, 110, D15309, doi:10.1029/2005JD005991, 2005.
469
470 Gerasopoulos, E., Kouvarakis, G., Vrekoussis, M., Donoussis, C., Mihalopoulos, N., M.,
471 Kanakidou: Photochemical ozone production in the Eastern Mediterranean. *Atm. Env.* 40, 3057–
472 3069, 2006a.
473
474 Gerasopoulos, E., Zanis, P., Papastefanou, C., Zerefos, C. S., Ioannidou, A., and Wernli, H.: A
475 complex case study of down to the surface intrusions of persistent stratospheric air over the
476 Eastern Mediterranean, *Atmos. Environ.*, 40, 4113–4125, 2006b.
477
478
479 Grell, G. A., Peckham, S. E., Schmitz, R., McKeen, S. A., Frost, G., Skamarock, W. C., and
480 Eder, B.: Fully coupled “online” chemistry within the WRF model, *Atmos. Environ.*, 39, 6957–
481 6975, 2005.
482
483 Guenther, A., Karl, T., Harley, P., Wiedinmyer, C., Palmer, P. I., and Geron, C.: Estimates of
484 global terrestrial isoprene emissions using MEGAN (Model of Emissions of Gases and Aerosols
485 from Nature), *Atmos. Chem. Phys.*, 6, 3181–3210, 2006. [http://www.atmos-chem-](http://www.atmos-chem-phys.net/6/3181/2006/)
486 [phys.net/6/3181/2006/](http://www.atmos-chem-phys.net/6/3181/2006/)
487
488 Hess, P. G. and Zbinden, R.: Stratospheric impact on tropospheric ozone variability and trends:
489 1990–2009, *Atmos. Chem. Phys.*, 13, 649–674, doi:10.5194/acp-13-649-2013, 2013.
490
491 Hijioka, Y., Matsuoka, Y., Nishimoto, H., Matsui, M., Kanuma, M.: Global GHG emissions
492 scenarios under GHG concentration stabilization targets, *Journal of Global Environmental*
493 *Engineering* 13, 97-108, 2008.
494
495 Hjellbrekke, A., Solberg, S. and Fjæraa, A.M. : Ozone measurements 2010 EMEP/CCC-Report
496 2/2012, available at: <http://www.nilu.no/projects/ccc/reports/cccr2-2012.pdf> (last access: 13
497 May 2014), 2012.
498
499 Hodnebrog, Ø., Solberg, S., Stordal, F., Svendby, T. M., Simpson, D., Gauss, M., Hilboll, A.,
500 Pfister, G. G., Turquety, S., Richter, A., Burrows, J. P., and Denier van der Gon, H. A. C.: Impact
501 of forest fires, biogenic emissions and high temperatures on the elevated Eastern Mediterranean
502 ozone levels during the hot summer of 2007, *Atmos. Chem. Phys.*, 12, 8727-8750,
503 doi:10.5194/acp-12-8727-2012, 2012.

504

505 Hauglustaine, D. A. and Brasseur, G. P.: Evolution of tropospheric ozone under anthropogenic
506 activities and associated radiative forcing of climate, *J. Geophys. Res.-Atmos.*, 106, 32337–
507 32360, doi:10.1029/2001jd900175, 2001.

508
509 Holton, J. R., Haynes, P. H., McIntyre, E. M., Douglass, A. R., Rood, R. B., and Pfister, L.:
510 Stratosphere-troposphere exchange, *Rev. Geophys.*, 33, 403–439, 1995.

511
512 Hurtmans D., Coheur P.-F., Wespes C., Clarisse L., Scharf O., Clerbaux C., Hadji-Lazaro J.,
513 George M., Turquety S.: FORLI radiative transfer and retrieval code for IASI, *Journal of*
514 *Quantitative Spectroscopy and Radiative Transfer* 113, 11, 1391-1408, 2012.

515
516 Im, U., Markakis, K., Poupkou, A., Melas, D., Unal, A., Gerasopoulos, E., Daskalakis, N.,
517 Kindap, T., and Kanakidou, M.: The impact of temperature changes on summer time ozone and
518 its precursors in the Eastern Mediterranean, *Atmos. Chem. Phys.*, 11, 3847–3864,
519 doi:10.5194/acp-11-3847-2011, 2011.

520
521 Kalabokas, P. D. and Bartzis, J. G.: Photochemical air pollution characteristics at the station of
522 the NCSR-Demokritos, during the MEDCAPHOT-TRACE campaign in Athens, Greece (20
523 August 20 September 1994), *Atmos. Environ.*, 32, 2123–2139, doi:10.1016/s1352-
524 2310(97)00423-8, 1998.

525
526
527 Kalabokas, P. D., Viras, L. G., Bartzis, J. G., and Repapis, C. C.: Mediterranean rural ozone
528 characteristics around the urban area of Athens, *Atmos. Environ.*, 34, 5199–5208,
529 doi:10.1016/s1352-2310(00)00298-3, 2000.

530
531 Kalabokas, P. D., Volz-Thomas, A., Brioude, J., Thouret, V., Cammas, J.-P., and Repapis, C. C.:
532 Vertical ozone measurements in the troposphere over the Eastern Mediterranean and comparison
533 with Central Europe, *Atmos. Chem. Phys.*, 7, 3783–3790, doi:10.5194/acp-7-3783-2007, 2007.

534
535 Kalabokas, P. D., Cammas, J.-P., Thouret, V., Volz-Thomas, A., Boulanger, D., and Repapis, C.
536 C.: Examination of the atmospheric conditions associated with high and low summer ozone
537 levels in the lower troposphere over the eastern mediterranean, *Atmos. Chem. Phys.*, 13, 10339–
538 10352, doi:10.5194/acp-13-10339-2013, 2013.

539
540 Kouvarakis, G., Tsigaridis, K., Kanakidou, M., and Mihalopoulos, N.: Temporal variations of
541 surface regional background ozone over Crete Island in the southeast Mediterranean, *J. Geophys.*
542 *Res.*, 105, 4399–4407, 2000.

543
544 Lamarque, J.-F., Hess, P. G., Emmons, L., Buja, L., Washington, W., and Granier, C.:
545 Tropospheric ozone evolution between 1890 and 1990, *J. Geophys. Res.*, 110, D08304, doi:
546 10.1029/2004JD005537, 2005.

547
548 Lelieveld, J., Berresheim, H., Borrmann, S., Crutzen, P. J., Dentener, F. J., Fischer, H., Feichter,
549 J., Flatau, P. J., Heland, J., Holzinger, R., Kormann, R., Lawrence, M. G., Levin, Z., Markowicz,

550 K. M., Mihalopoulos, N., Minikin, A., Ramanathan, V., de Reus, M., Roelofs, G. J., Scheeren, H.
551 A., Sciare, J., Schlager, H., Schultz, M., Siegmund, P., Steil, B., Stephanou, E. G., Stier, P.,
552 Traub, M., Warneke, C., Williams, J., and Ziereis, H.: Global air pollution crossroads over the
553 mediterranean, *Science*, 298, 794–799, doi:10.1126/science.1075457, 2002.

554
555 Liu, J., Jones, D. B. A., Zhang, S., and Kar, J.: Influence of interannual variations in transport on
556 summertime abundances of ozone over the Middle East, *J. Geophys. Res.*, 116, D20310,
557 doi:10.1029/2011JD016188, 2011.

558
559 Ma, J., Zhou, X., and Hauglustaine, D.: Summertime tropospheric ozone over China simulated
560 with a regional chemical transport model, Part 2. Source contribution and budget, *J. Geophys.*
561 *Res.*, 107 (D22), 4612, doi:10.1029/2001JD001355, 2002.

562
563 Papayannis, A., Balis, D., Zanis, P., Galani, E., Wernli, H., Zerefos, C., Stohl, A., Eckhardt, S.,
564 and Amiridis, V.: Sampling of an STT event over the Eastern Mediterranean region by lidar and
565 electrochemical sonde, *Ann. Geophys.*, 23, 2039–2050, doi:10.5194/angeo-23-2039-2005, 2005.

566
567 Pfister, G., Emmons, L. K., Hess, P. G., Honrath, R., Lamarque, J.-F., Val Martin, M., Owen, R.
568 C., Avery, M., Browell, E. V., Holloway, J. S., Nedelec, P., Purvis, R., Rywerson, T. B., Sachse,
569 G. W., and Schlager, H.: Ozone production from the 2004 North American boreal fires, *J.*
570 *Geophys. Res.*, 111, D24S07, doi:10.1029/2006JD007695, 2006.

571
572 Pfister, G. G., Emmons, L. K., Hess, P. G., Lamarque, J.-F., Thompson, A. M., and Yorks, J. E.:
573 Analysis of the summer 2004 ozone budget over the United States using Intercontinental
574 Transport Experiment Ozone Sonde Network Study (IONS) observations and Model of Ozone and
575 Related Tracers (MOZART-4) simulations, *J. Geophys. Res.*, 113, D23306,
576 doi:10.1029/2008JD010190, 2008.

577
578 Pfister, G. G., Walters, S., Emmons, L. K., Edwards, D. P., and Avise, J.: Quantifying the
579 contribution of inflow on surface ozone over California during summer 2008, *J. Geophys. Res.*
580 *Atmos.*, 118, 12,282–12,299, doi:10.1002/2013JD020336, 2013.

581
582 R'Honi, Y., Clarisse, L., Clerbaux, C., Hurtmans, D., Dufлот, V., Turquety, S., Ngadi, Y., and
583 Coheur, P.-F.: Exceptional emissions of NH₃ and HCOOH in the 2010 Russian wildfires, *Atmos.*
584 *Chem. Phys.*, 13, 4171-4181, doi:10.5194/acp-13-4171-2013, 2013.

585
586 Richards, N. A. D., Arnold, S. R., Chipperfield, M. P., Miles, G., Rap, A., Siddans, R.,
587 Monks, S. A., and Hollaway, M. J.: The Mediterranean summertime ozone maximum: global
588 emission sensitivities and radiative impacts, *Atmos. Chem. Phys.*, 13, 2331-2345,
589 doi:10.5194/acp-13-2331-2013, 2013.

590
591 Rodwell, M. J. and Hoskins, B. J.: Monsoons and the dynamics of deserts, *Q. J. R. Meteorol.*
592 *Soc.*, 122, 1385–1404, doi:10.1002/qj.49712253408, 1996.

593
594 Rodwell, M. J. and Hoskins, B. J.: Subtropical anticyclones and summer monsoons, *J. Climate*,
595 14, 3192–3211, 2001

596 Roelofs, G. J., Scheeren, H. A., Heland, J., Ziereis, H., and Lelieveld, J.: A model study of ozone
597 in the eastern Mediterranean free troposphere during MINOS (August 2001), *Atmos. Chem.*
598 *Phys.*, 3, 1199–1210, doi:10.5194/acp-3-1199-2003,
599 2003.
600

601 Safieddine S., Clerbaux C., George M., Hadji-Lazaro J., Hurtmans D., Coheur P.-F., Wespes C.,
602 Loyola D., Valks P., Hao N.: Tropospheric ozone and nitrogen dioxide measurements in urban
603 and rural regions as seen by IASI and GOME-2, *J. Geo. Phys. Res : Atmospheres* 118, 18, 10555-
604 10566, 2013.
605

606 Schubert, S., Wang, H., and Suarez, M.: Warm season sub-seasonal variability and climate
607 extremes in the Northern Hemisphere: the role of stationary Rossby waves. *J. Climate*, 24, 4773-
608 4792, 2011.
609

610 Sprenger, M. and Wernli, H.: A northern hemispheric climatology of cross-tropopause exchange
611 for the ERA15 time period 1979–1993), *J. Geophys. Res.*, 108, 8521,
612 doi:10.1029/2002JD002636, 2003.
613

614 Stohl, A., Spichtinger-Rakowsky, N., Bonasoni, P., Feldmann, H., Memmesheimer, M., Scheel,
615 H. E., Trickl, T., Hubener, S. H., Ringer, W., and Mandl, M.: The influence of stratospheric
616 intrusions on alpine ozone concentrations, *Atmos. Environ.*, 34,1323–1354, 2000.
617

618 Tuccella, P., Curci, G., Visconti, G., Bessagnet, B., Menut, L., and Park, R. J.: Modeling of gas
619 and aerosol with WRF/Chem over Europe: Evaluation and sensitivity study, *J. Geophys. Res.*,
620 117, D03303, doi:10.1029/2011JD016302, 2012.
621

622 Turquety, S., Hurtmans, D., Hadji-Lazaro, J., Coheur, P.-F., Clerbaux, C., Josset, D., and
623 Tsamalis, C.: Tracking the emission and transport of pollution from wildfires using the IASI CO
624 retrievals: analysis of the summer 2007 Greek fires, *Atmos. Chem. Phys.*, 9, 4897–4913, 2009,
625 <http://www.atmos-chem-phys.net/9/4897/2009/>.
626

627 Tyrllis, E., Lelieveld, J., and Steil, B.: The summer circulation in the eastern Mediterranean and
628 the Middle East: influence of the South Asian Monsoon, *Clim. Dynam.*, 40, 1103–1123,
629 doi:10.1007/s00382-012-1528-4, 2013a.
630

631 Wespes, C., Emmons, L., Edwards, D. P., Hannigan, J., Hurtmans, D., Saunio, M., Coheur, P.-
632 F., Clerbaux, C., Coffey, M. T., Batchelor, R. L., Lindenmaier, R., Strong, K., Weinheimer, A. J.,
633 Nowak, J. B., Ryerson, T. B., Crounse, J. D., and Wennberg, P. O.: Analysis of ozone and nitric
634 acid in spring and summer Arctic pollution using aircraft, ground-based, satellite observations
635 and MOZART-4 model: source attribution and partitioning, *Atmos. Chem. Phys.*, 12, 237-259,
636 doi:10.5194/acp-12-237-2012, 2012.

637 Wiedinmyer, C., Akagi, S. K., Yokelson, R. J., Emmons, L. K., Al-Saadi, J. A., Orlando, J. J.,
638 and Soja, A. J.: The Fire Inventory from NCAR (FINN) – a high resolution global model to
639 estimate the emissions from open burning, *Geosci. Model Dev.*, 4, 625–641, 2011.
640

641 Zanis, P., Hadjinicolaou, P., Pozzer, A., Tyrlis, E., Dafka, S., Mihalopoulos, N., and Lelieveld, J.:
 642 Summertime free-tropospheric ozone pool over the eastern Mediterranean/Middle East, *Atmos.*
 643 *Chem. Phys.*, 14, 115-132, doi:10.5194/acp-14-115-2014, 2014.

644
 645 Zbinden, R. M., Thouret, V., Ricaud, P., Carminati, F., Cammas, J.-P., and Nédélec, P.:
 646 Climatology of pure tropospheric profiles and column contents of ozone and carbon monoxide
 647 using MOZAIC in the mid-northern latitudes (24° N to 50° N) from 1994 to 2009, *Atmos. Chem.*
 648 *Phys.*, 13, 12363-12388, doi:10.5194/acp-13-12363-2013, 2013.

649
 650 Ziv, B., Saaroni, H., and Alpert, P.: The factors governing the summer regime of the Eastern
 651 Mediterranean, *Int. J. Climatol.*, 24, 1859–1871, 2004

652
 653
 654
 655

656 Table 1: List of geographic location of the EMEP O₃ monitoring ground stations used in this
 657 study, with the corresponding altitude above mean sea level.

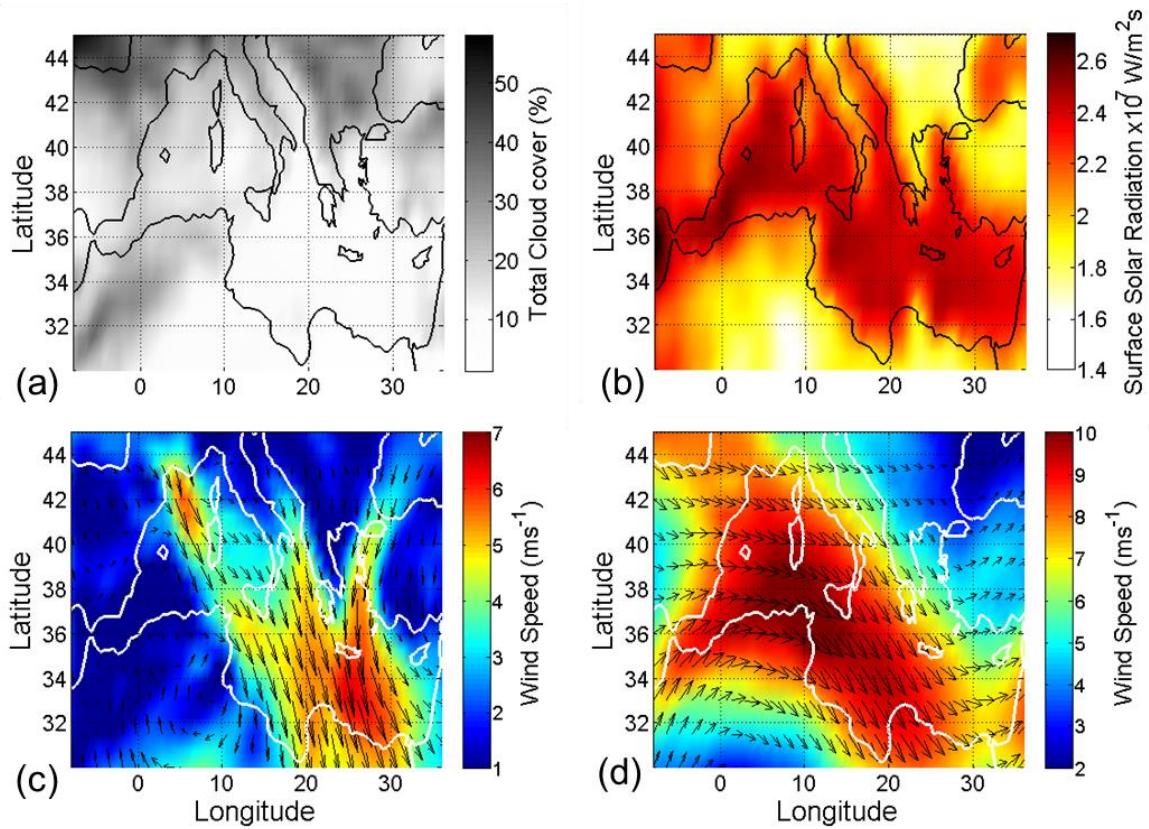
658

Code	Station name	Latitude (°N)	Longitude (°E)	Altitude (m)
CY02	Ayia Marina	35.04	33.06	532
ES06	Mahón	39.87	4.32	78
ES07	Víznar	37.30	-3.53	1265
ES10	Cabo de Creus	42.32	3.32	23
ES12	Zarra	39.08	-1.10	885
ES14	Els Torms	41.39	0.73	470
GR02	Finokalia	35.31	25.66	250
MK07	Lazaropole	41.32	20.42	1332

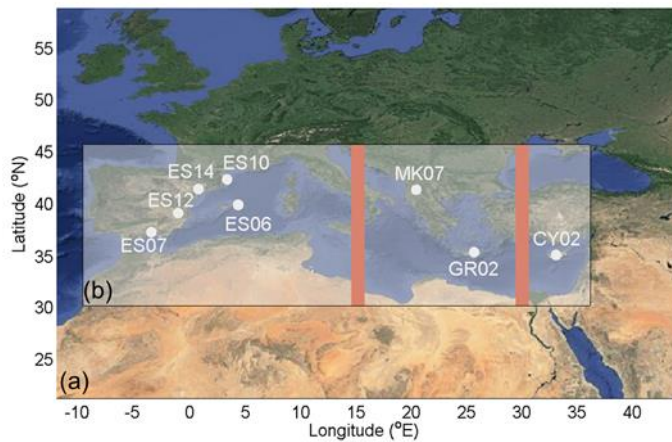
659
 660
 661 Table 2. Pearson correlation coefficient, bias and the corresponding mean normalized bias
 662 (MNB) of each EMEP and WRF-Chem ground station data localized in Fig. 2, for the period JJA
 663 2010.

Station name	Corr. Coef. With WRF-Chem	Bias (ppbv)	MNB (%)
CY02	0.63	-7.78	(-14.2%)
ES06	0.41	+7.26	(+20.9%)
ES07	0.77	-7.24	(-13.4%)
ES10	0.72	+1.43	(+3.6%)
ES12	0.80	-5.96	(-12.7%)
ES14	0.78	-2.99	(-6.4%)
GR02	0.62	-7.38	(-11.3%)
MK07	0.57	-16.65	(-23.9%)

664
 665
 666



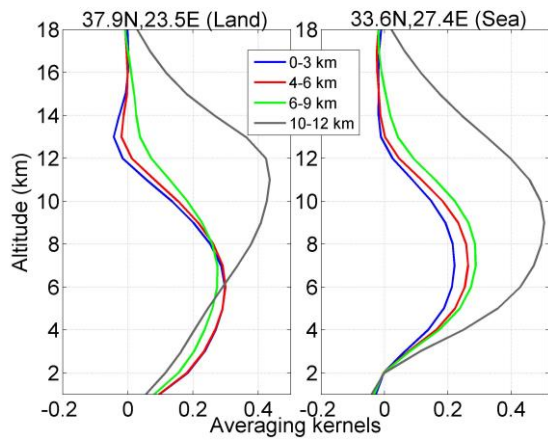
667
 668 **Fig.1.** An example of the ECMWF (European Centre for Medium-Range Weather Forecasts)
 669 Reanalysis (ERA-Interim) for the period June-July-August (JJA) 2010 for: (a) total cloud
 670 coverage, (b) 12:00 UTC solar radiation reaching the surface and (c) wind speed and direction
 671 averaged from the surface to 750 hPa and (d) wind speed and direction averaged from 750 to 400
 672 hPa.



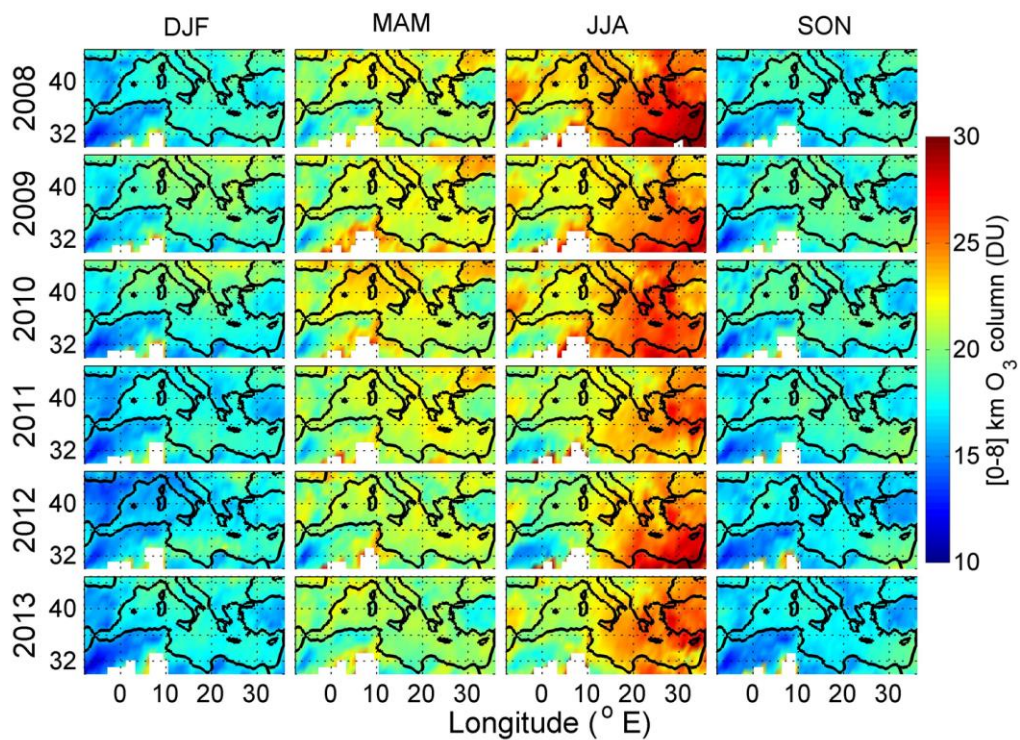
673

24

674 **Fig. 2.** (a) The enlarged WRF-Chem model run domain. (b) IASI and WRF-Chem domain used
675 in this study. White dots correspond to the location of the EMEP ground stations and the orange
676 strips correspond to the longitudinal transects used in Figures 5 and 10.
677

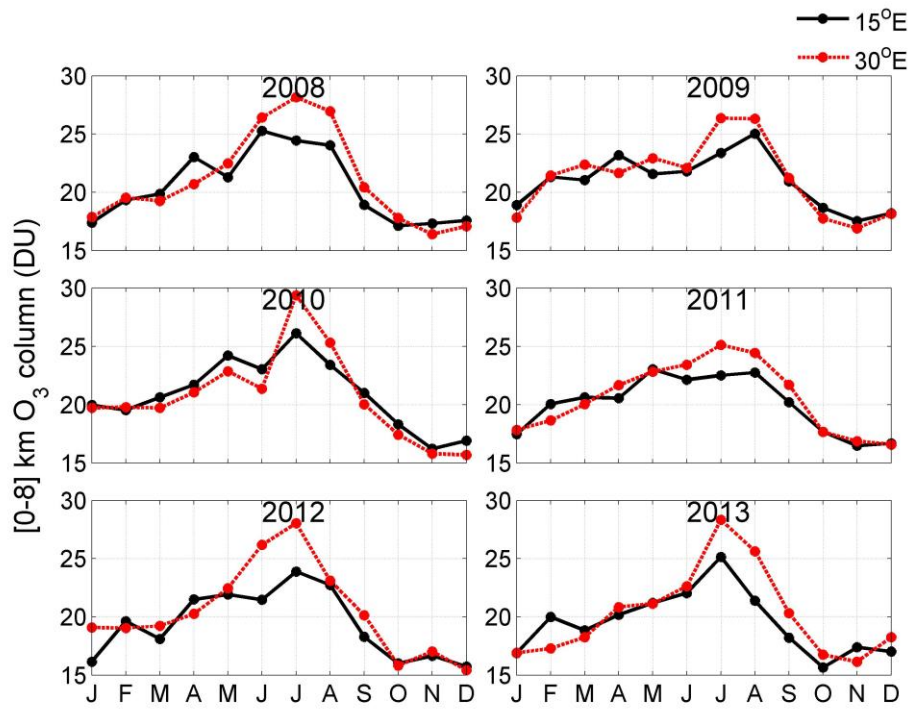


678
679 **Fig. 3.** Random O₃ averaging kernels over the Mediterranean: the functions are for the [surface-
680 3], [4-6], [6-9], and [10-12] km partial columns characterizing a retrieval for an observation
681 chosen randomly above land (Greece, left panel) and above the sea (right panel) during June
682 2010.



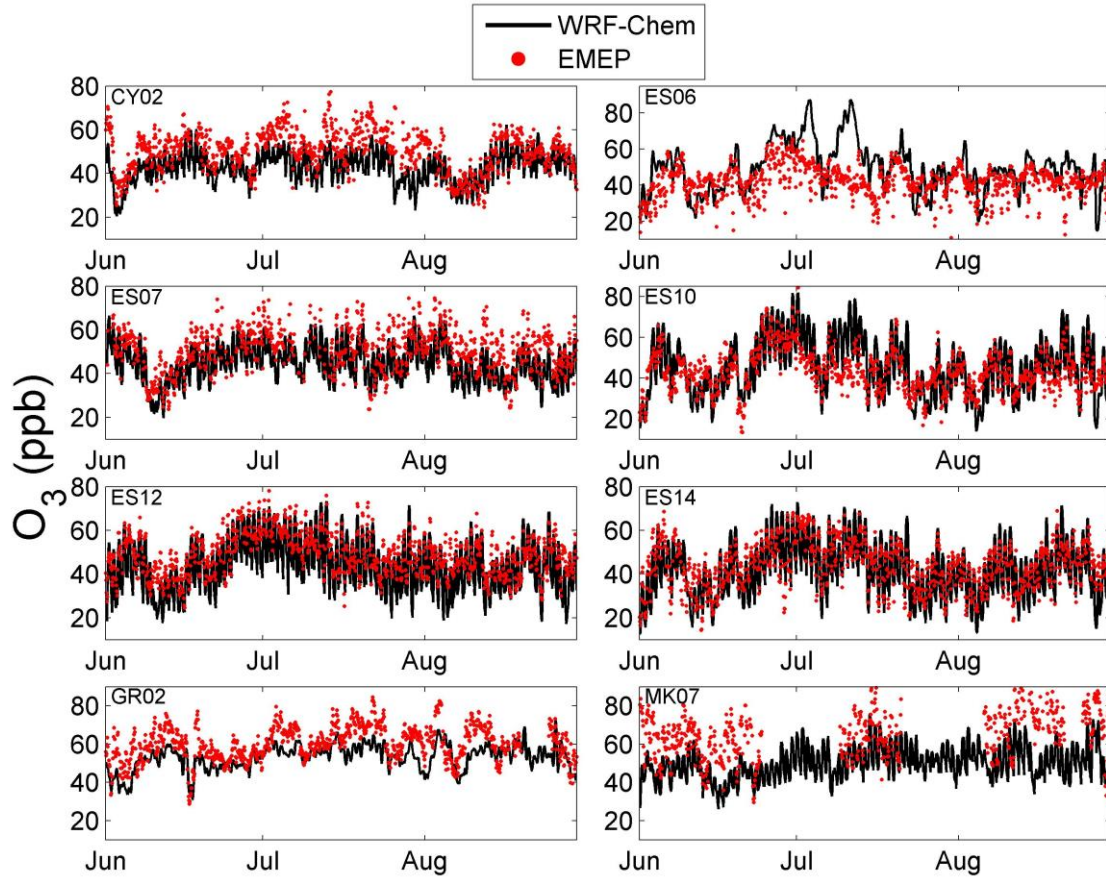
683

684 **Fig. 4.** Six years seasonal variation of [0-8] km integrated IASI O₃ column over the
 685 Mediterranean region for winter, spring, summer and autumn. White pixels correspond to a filter
 686 applied on poor spectral fits, because of emissivity issues in the FORLI radiative transfer above
 687 the Sahara desert.

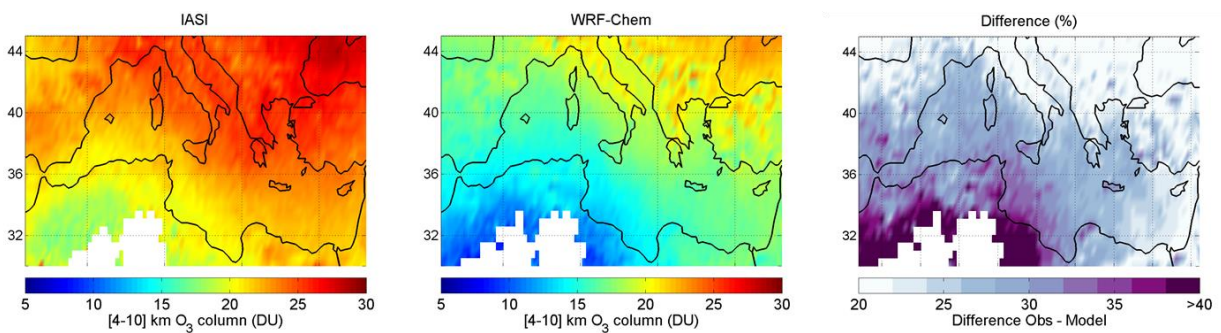


688
 689 **Fig. 5.** Six years monthly variation of the integrated [0-8] km IASI O₃ column averaged over
 690 [30°N-45°N] at 15°E (in black) and 30°E (in red). Higher summer values are observed to the east
 691 of the basin at 30°E.

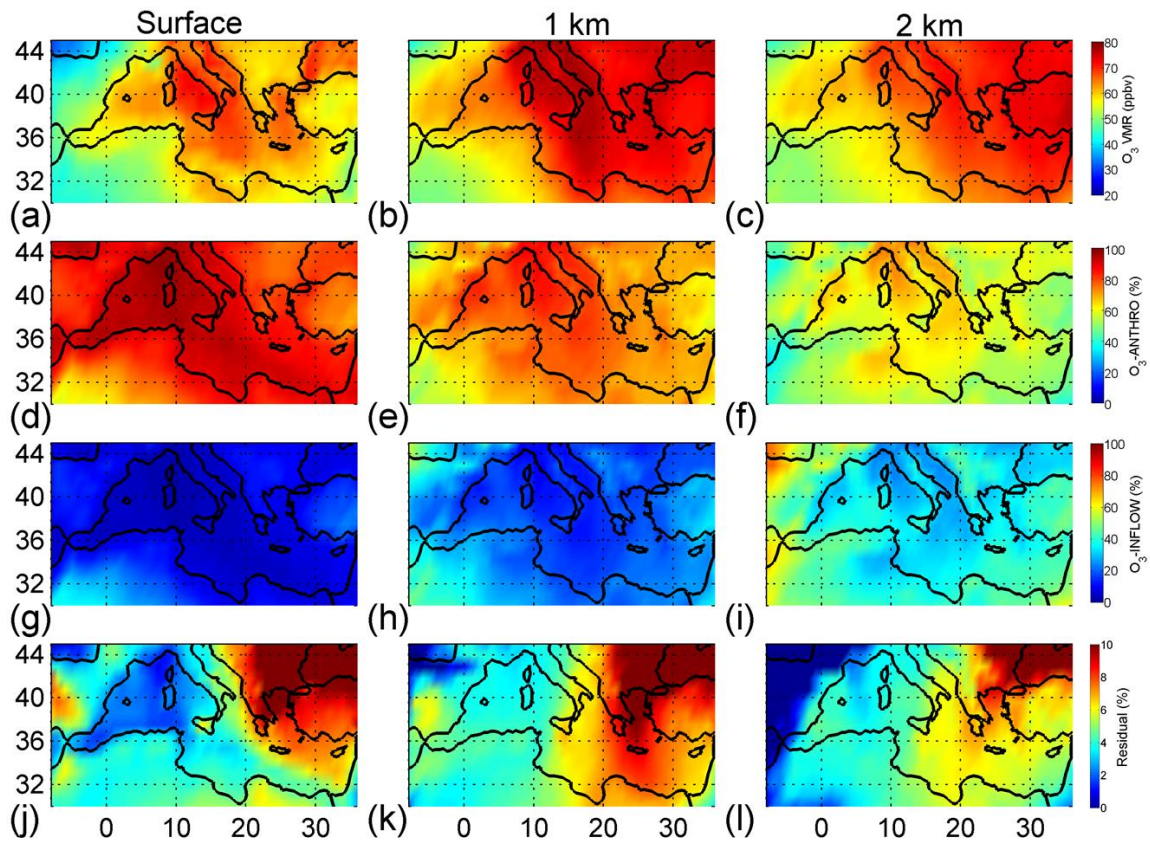
692
 693
 694
 695



696
 697 **Fig. 6.** O₃ time series of EMEP and WRF-Chem data at the surface for the stations localized in
 698 Fig. 2, for the period JJA 2010.



699
 700 **Fig. 7.** Average [4-10] km O₃ column for JJA 2010 from IASI and WRF-Chem and their relative
 701 difference (%). White pixels correspond to a filter applied to poor spectral fits above the Sahara
 702 desert.



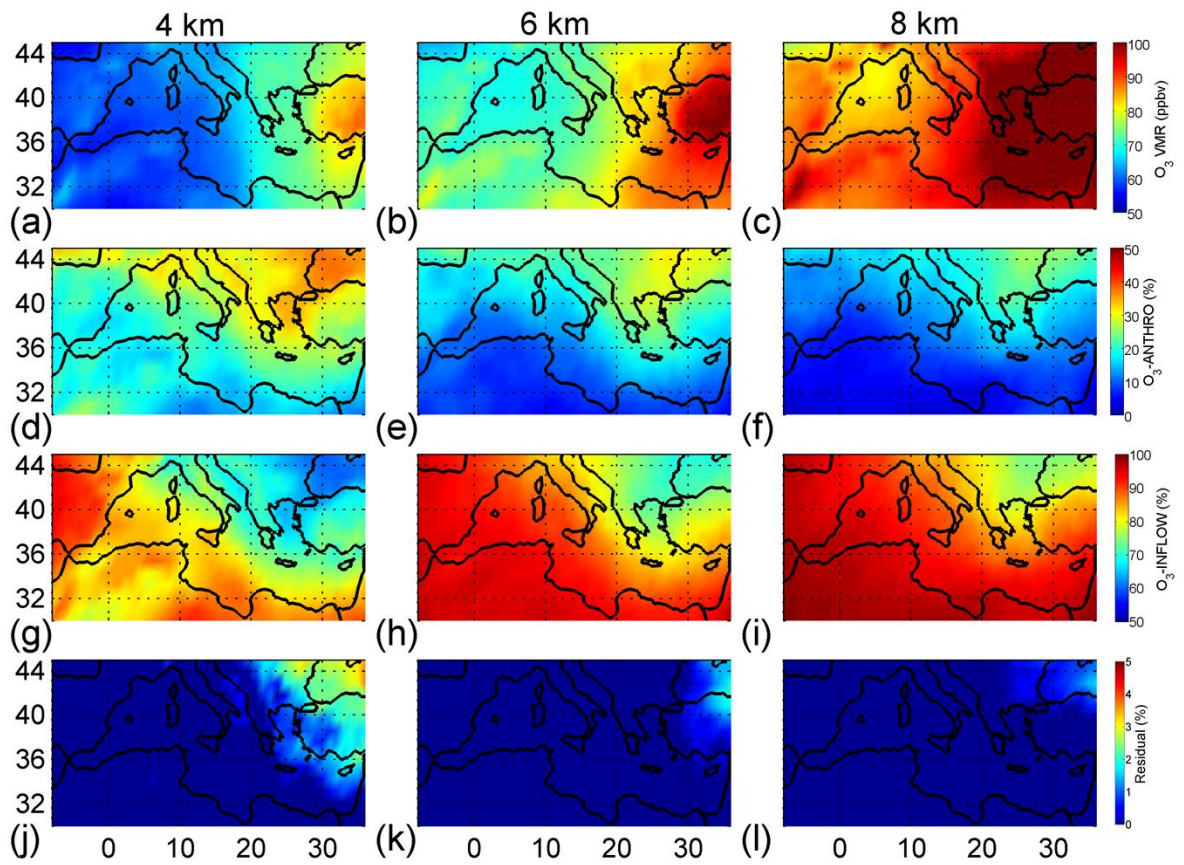
703

704 **Fig. 8.** WRF-Chem spatial distributions of (a-c) O₃ mixing ratios (ppbv), (d-f) O₃ anthropogenic

705 tracer relative contributions (%), (g-i) O₃ inflow tracer relative contribution, and (j-l) the residual

706 $(100\% - (O_{3-ANTHRO}\% + O_{3-INFLOW}\%))$ averaged over the period JJA 2010 at the surface, 1 km and 2

707 km. Note that the colorbar for the residual plots is different.

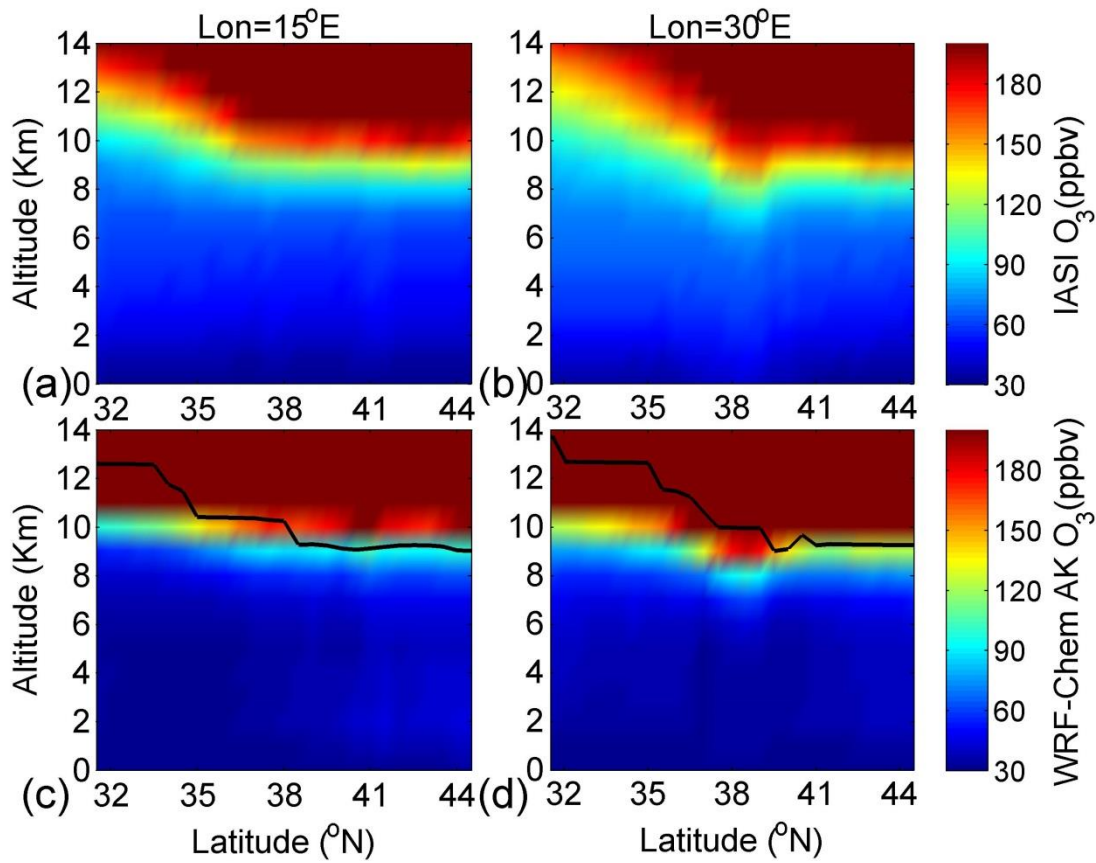


708

709 **Fig. 9.** Same as Fig. 8 but for 4, 6 and 8 km.

710

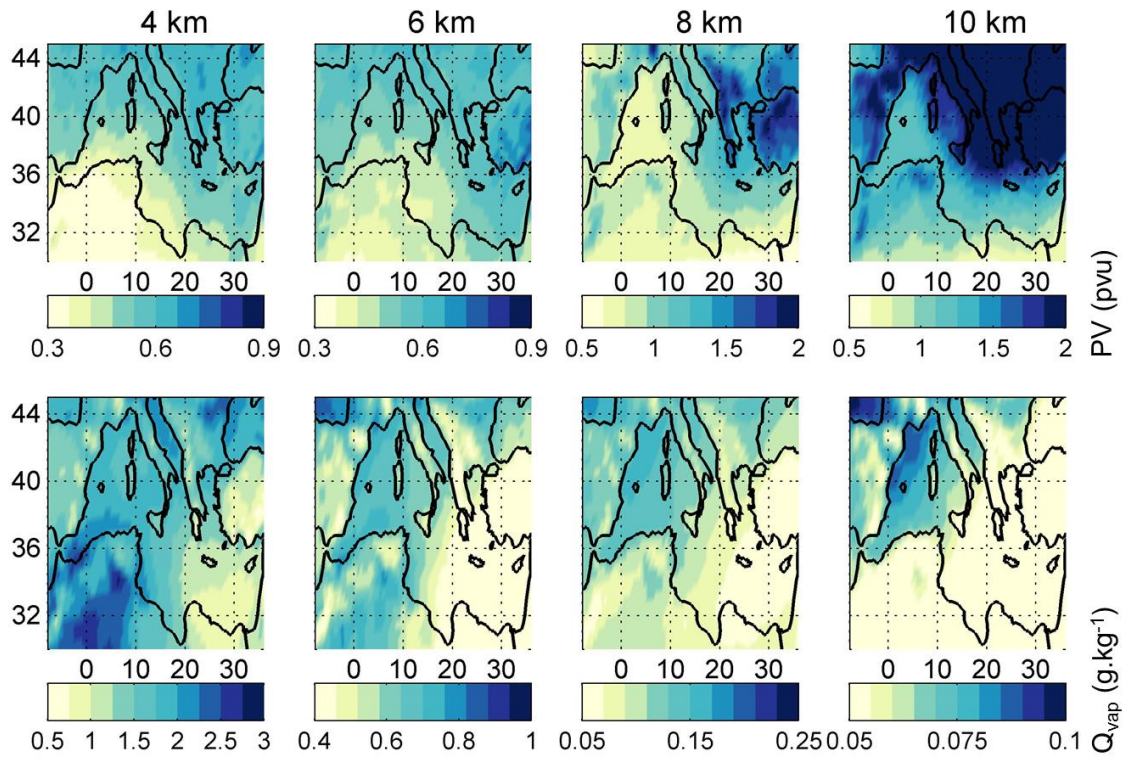
711



712

713 **Fig.10.** Mean latitude-altitude cross sections of IASI-O₃ (a-b) and modeled-O₃ (c-d) averaged
 714 over JJA 2010 at 15°E (left) and 30°E (right). Black line corresponds to the dynamical tropopause
 715 height.

716



717

718 **Fig. 11.** WRF-Chem (a) potential vorticity (PV) at 4, 6, 8 and 10 km over the Mediterranean
 719 region for JJA 2010 and (b) water vapor mixing ratio (Q_{vap}) for the same vertical levels and time
 720 period.

721